

FATIGUE CHARACTERIZATION OF ULTRASONIC ADDITIVE MANUFACTURED ALUMINUM 3003

P.J. Wolcott and M.J. Dapino

Department of Mechanical and Aerospace Engineering, The Ohio State University, Columbus, OH, 43210

Abstract

An aluminum 3003 H-18 block was built using ultrasonic additive manufacturing with process parameters which optimize mechanical strength. Transverse tensile fatigue tests were conducted on samples cut from the block and a stress vs. number of cycles curve was generated. Results show the curve is relatively flat and a stress threshold of 50% of the ultimate transverse tensile strength exists below which failure does not occur within 3.75×10^7 cycles. Optical and scanning electron microscopy conducted on failure surfaces shows no signs of crack initiation or growth typical of fatigue loading, but exhibits areas of no bonding between foil layers. To explain the failure, a model was developed based on the probabilistic failure of bonded areas in tension. The model uses a Frechet distribution to describe the probability of failure at each individual bonded area. Discrete bond failure and subsequent redistribution of stress to the surviving areas eventually leads to failure for the entire sample. Predictions from the model show good correlation with the experimental results.

Introduction

Ultrasonic additive manufacturing (UAM), also known as ultrasonic consolidation, is a solid state manufacturing process that joins layered metal foils using principles of ultrasonic metal welding in combination with subtractive milling processes to create near net shape metal parts [1]. The process uses a rolling sonotrode to apply ultrasonic vibrations to metal foils; the scrubbing action produced by the sonotrode breaks up oxides and contaminants on the surface of the adjacent foil layers generating nascent bond surfaces. Normal force applied via the sonotrode creates intimate metal to metal contact between the nascent surfaces which results in metallic bonding well below the foil melting temperature [2]. Heat generation due to the scrubbing action ranges from 30% to 50% of the foil melting temperature [3]. Therefore, UAM provides unprecedented opportunities to manufacture metal-matrix composites with embedded elements such as smart materials and electronics that are normally sensitive to thermal cycling [4] [5]. Input parameters of tack force, weld force, weld rate, amplitude and preheat temperature can be adjusted depending on the foil material to maximize the bonding and mechanical strength between foil layers [6].

To realize the entire potential of UAM, it is necessary to fully characterize the mechanical properties of UAM builds. Several studies have utilized microstructure, peel strength or void density analyses to understand the relationship between bond quality and manufacturing parameters, focusing mainly on aluminum 3003 as the foil material [7] [8] [9]. These tests provide valuable information on the bonding characteristics of UAM builds, but are difficult to correlate to common mechanical strength properties. Studies by Hopkins et al. [6] [10] have

determined optimal sets of parameters for various material combinations based on mechanical strength testing, including transverse tensile and shear strength. These tests provide a direct comparison to the mechanical properties of traditionally manufactured metal structures. Specifically, transverse tensile tests provide an indication of the strength at the interface with the lowest bond strength.

Fatigue characterization of UAM built structures is important to determine potential lifetimes in cyclic loading conditions for structures in service. Up to this point, fatigue analyses of UAM built structures have not been available in the literature. The fatigue testing presented here will provide the first such lifetime prediction data for the design of UAM components.

Experimental Procedure

Sample Fabrication

A UAM block with dimensions 101.6 mm x 50.8 mm x 33 mm (4 in. x 2 in. x 1.3 in.) was fabricated using a Solidica, Inc. Beta UAM machine (2 kW) at Edison Welding Institute, Columbus, Ohio from which fatigue samples were cut. The block consisted of Al 3003 H-18 foils, 152.4 μm thick (0.006 in.) built upon a 12.7 mm (0.5 in.) thick Al 3003 H-14 baseplate. Joining of successive foil layers was accomplished through tacking and welding passes; the input energy in the welding pass was higher than in the tacking pass. A staggered, alternating layup of foils was used to eliminate seams running through the height of the build. In addition, milling passes were conducted periodically throughout the building process to maintain flatness. Samples were cut from the block via wire electronic discharge machining avoiding any seams and machined via CNC lathe to the specified dimensions shown in Figure 1. Sample dimensions include 12.7 mm baseplate material to more closely follow dimensional requirements in ASTM standard E466-7 for conducting axial loaded fatigue tests [11].

The process parameters used for the build are given in Table 1. The parameters chosen were based on a study by Hopkins et al. [10] that determined optimal process parameters for mechanical strength of UAM Al 3003 H-18 builds on the Solidica Inc. Beta UAM machine. These parameters provide an ultimate shear strength of approximately 22 MPa and an ultimate transverse tensile strength (UTTS) of approximately 30 MPa when using Al 3003 H-18 foils.

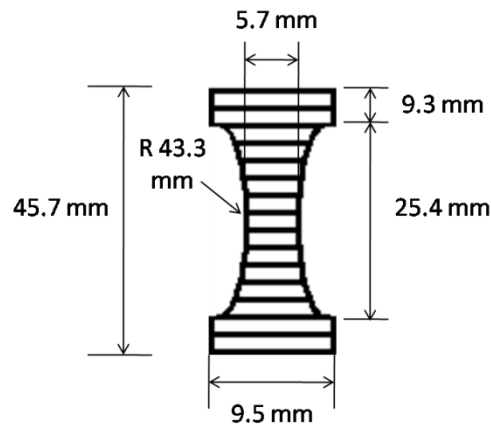


Figure 1 - Sample dimensions for transverse axial fatigue testing (foils not to scale).

Table 1 - Process parameters for UAM build.

Tack Force	350 N
Weld Force	1000 N
Amplitude	26 μm
Weld Rate	42 mm/s
Tack Rate	50.8 mm/s
Tack Amplitude	9 μm
Base Plate Temperature	150°C
Sonotrode Texture, R_a	7 μm
Oscillation Frequency	20 kHz

Sample Testing

Fatigue testing was conducted using principles outlined in ASTM standard E466-7 [11] in a MTS 831 test frame with 25 kN load capacity specially designed for high-cycle fatigue testing. Samples were loaded axially in tension with a minimum load of 22.24 N (5 lbs) to avoid compressive strokes that could affect fracture surfaces after failure. The R-ratio, given by,

$$R = \frac{\sigma_{min}}{\sigma_{max}} \quad (1)$$

was near zero for these tests. Loading was conducted transverse to the foil layup direction as seen in Figure 1. Since the transverse orientation is the lowest strength direction for UAM composites [12], it is necessary to study the fatigue behavior in this orientation. The cyclic tests were conducted using load control with the number of cycles counted until failure. The frequency of cycling for each test was ramped to 10 Hz within 100 cycles and sustained through 1.0×10^6 cycles. For samples tested beyond 1.0×10^6 cycles, the frequency was increased to 30 Hz to expedite the testing. This test procedure and the frequencies used are well within the standards and are commonly used for fatigue load cycling [11] [13]. After testing, all of the samples were examined via optical and scanning electron microscopy (SEM) to investigate the specimen failure surfaces for bonding and failure characteristics.

Experimental Results

The stress-number of cycles (S-N) curve showing the results of the fatigue testing is given in Figure 2. The plot shows the maximum stress vs. cycles to failure as well as the percentage of the UAM ultimate transverse tensile strength for each stress level. Samples were considered runouts when loaded to 3.75×10^7 cycles without failure; the three samples that reached this threshold are designated with arrows in Figure 2. Two of these samples were tested again at higher stress levels to maximize the number of tests in the study; these retests are represented with R on the figure.

Two samples which failed in unexpected ways were omitted from the results. In Figure 2, these outliers are indicated with circles around the data points. One of the samples failed along a mill line that was created due to the flattening passes during the build, seen in Figure 3(a). This

failure is attributed to a manufacturing defect caused due to mill pass creating a height difference along a build interface. Another sample failed near the first layer at the edge of the gauge region, seen in Figure 3(b), indicating that the first layer did not weld strongly to the baseplate. Since these failures arise from identifiable and atypical manufacturing issues, these two results are disregarded in the fatigue analysis.

Fatigue fracture surfaces for the samples that failed by delamination were similar to those found in [10] for UTTS samples; an example optical microscope image is shown in Figure 4. Images from the top foil layer of the delamination failure were utilized because they are not textured directly by the sonotrode during the building process, providing an ideal surface for bond characterization. The failure surface shows dark areas as original foil texture and lighter areas that have been textured by the foil layer it was bonded to. Important features not present in the optical microscopy are a clear crack initiation site and striations growing from this site. This indicates a need to look more closely at the failure surfaces using scanning electron microscopy.

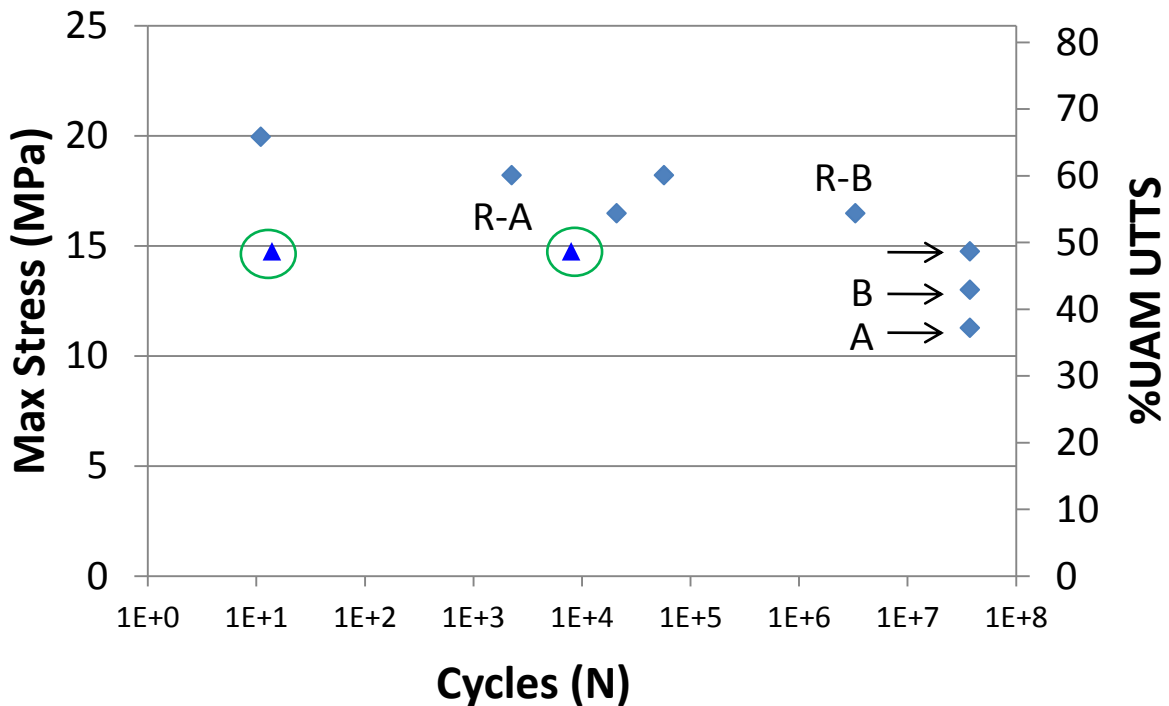
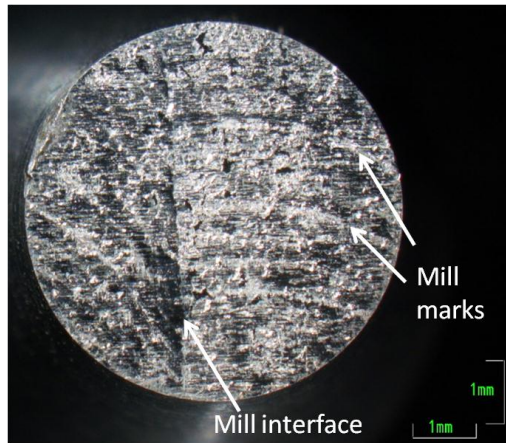


Figure 2 - Stress-cycle plot of maximum stress and cycles to failure. The arrows represent specimens that did not fail within 3.75×10^7 cycles and R represents samples retested at higher stress levels. Circled points represent samples that did not fail by delamination of foil layers.



(a)



(b)

Figure 3 - (a) Optical microscope image of sample failure along milling interface with mill marks shown; (b) Sample failure at edge of gauge region at the baseplate layer.

Example SEM micrographs in Figure 5 show areas of ductile failure typical of metallic bonding, areas of original foil texture indicating no bonding, and areas of foil to foil contact without bonding (designated as flow), each consistent with the optical and SEM results presented in [10]. These characteristics were present in all of the failure surfaces. The areas of original foil texture are seen in the images as flat and dark whereas the ductile areas are lighter in color with a cup-cone like structure. The areas of foil to foil contact without bonding are lightly colored as well but do not show the cup-cone structure. None of the optical or SEM microscopy analyses show the characteristics expected in a fatigue failure, such as a well-defined crack initiation site and fatigue striations showing the growth of an initial crack.

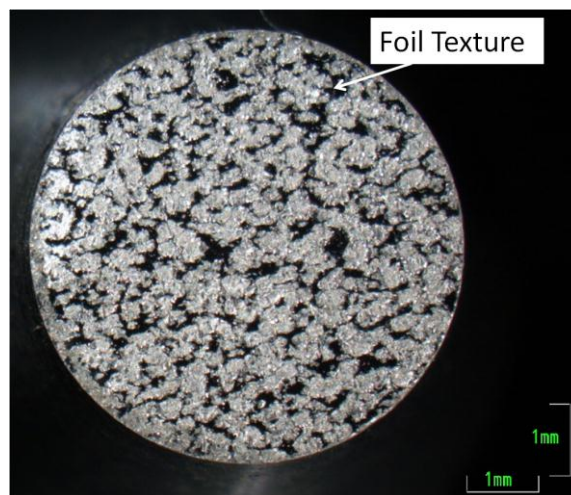


Figure 4 - Optical micrograph of fatigue fracture surface.

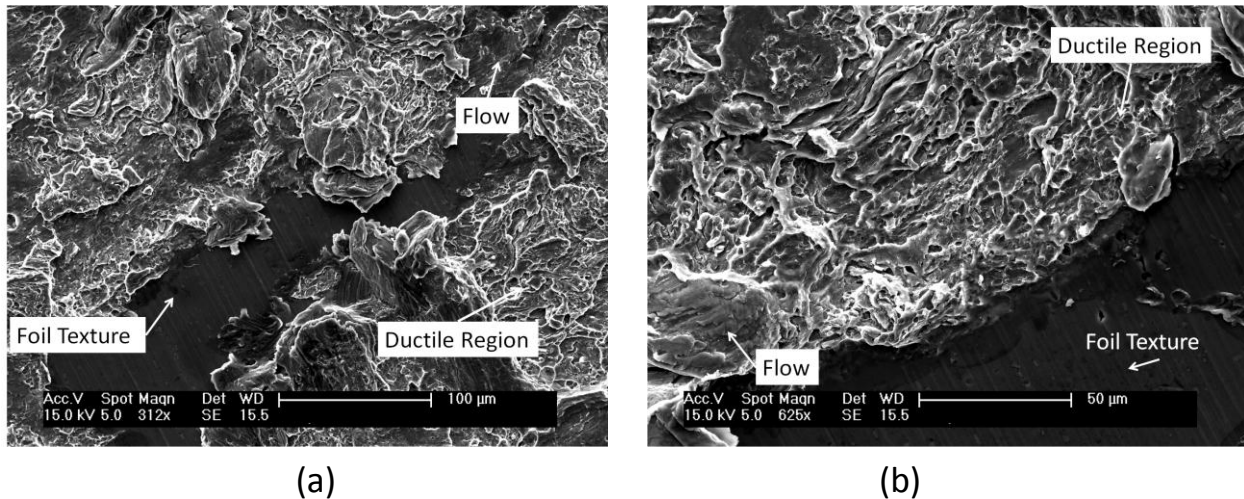


Figure 5 - SEM images of fatigue fracture surface showing ductility, foil to foil contact without bonding (flow), and original foil texture: (a) 312x and (b) 625x.

Discussion of Experimental Results

The S-N curve suggests that a threshold of approximately 50% of the UAM ultimate transverse tensile strength exists below which fatigue failure does not occur within 3.75×10^7 cycles. Because it is known that nonferrous metals such as aluminum do not have a fatigue limit, it is expected that UAM Al 3003 builds would fail eventually given sufficient cyclic loading. At 30 Hz, testing a sample to 3.75×10^7 cycles requires more than two weeks. For this reason, more stress cycling on the samples that ran out in this study was not conducted. The S-N curve for the UAM Al 3003 build is relatively flat with most samples failing in the range from 20 to 15 MPa. These results, in addition to the lack of classic fatigue characteristics indicate a need for alternate explanations for lifetime prediction of UAM samples. It is therefore necessary to investigate alternate explanations for the failure using scaled modeling efforts.

Model Development

The absence of classic fatigue features, such as a crack initiation site or striations, motivates the development of an alternate theory to describe the failure of UAM samples under dynamic loading conditions. The model developed in this case uses the concept of simultaneous tensile loads on the discrete bonded areas of a UAM build. As each loading cycle is applied, there is a probability of failure for each bond that, if failure conditions are met, can lead to failure of that bond and a redistribution of stress to the surviving bonded areas. Using a probability of failure approach incorporates the concepts of stress concentrations, stress buildup, and asymmetric loading conditions under one metric. Simulating the failure in this way avoids having to calculate each phenomenon individually with a complex stress analysis at each bond. This makes the model ideal as an initial test without being overburdened with unknown factors. Figure 6 shows a side view schematic of the bonding illustrating the model theory, whereby on each load cycle there is a possibility of bond failure.

The evolution of stress on the bonds is described by,

$$\sigma = \frac{F_0}{\gamma * A_0 * x} = \frac{\sigma_0}{x} \quad (2)$$

where F_0 is the nominal load applied, A_0 is the nominal area of the sample (not accounting for actual bonding), γ is the percentage of actual bonding present prior to loading (18.1% [10]), and x is the percentage of surviving bonds starting at an initial value of 100% without any load cycling and 0% at failure. This equation therefore scales the stress based on the amount of bonding present during the loading. The model uses a set of random numbers checked against the probability of failure curve to determine whether a bond is to fail or not. In this case a random number from 0-1 is checked against the probability curve at the loading stress. If the random number is less than the probability of failure at a given stress level, the bond is deemed to have failed and its value becomes zero.

For simplicity, the bonding was assumed to be 100 equally sized areas. The value for x is the sum of a 100 index vector, each initialized with a value of 1/100. As the bonds fail, corresponding indices are reset to 0, changing the sum of the vector to a value less than 1. This in turn decreases the number of surviving bonds, x , and therefore the stress increases according to equation (2). This process is continued until a condition is met where $\sigma \geq \sigma_{UTS}$, where σ_{UTS} is the ultimate tensile strength of the wrought Al 3003-H18 alloy (200 MPa) [14]. When failure occurs, the number of cycles is reported as the final value for the fatigue life at the given initial stress. The use of random numbers and the range of probabilities of failure build considerable variation into the model to simulate the stochastic nature of UAM bonding and failure.

The probability of failure curves were fit from the experimental results based on a Fréchet distribution given by,

$$F(V) = \exp \left[- \left(\frac{s}{\sigma - \sigma_0} \right)^\alpha \right] \quad (3)$$

where s is a scale parameter, σ_0 is a location parameter, and α is a shape parameter [15]. The model parameters for the failure probability are given in Table 2 and the curves used for the model are given in Figure 7. Two curves were generated using two values of σ_0 to simulate the stochastic nature of the bonding in UAM structures. In the model, the value of the probability of failure is selected as a random value between the two curves.

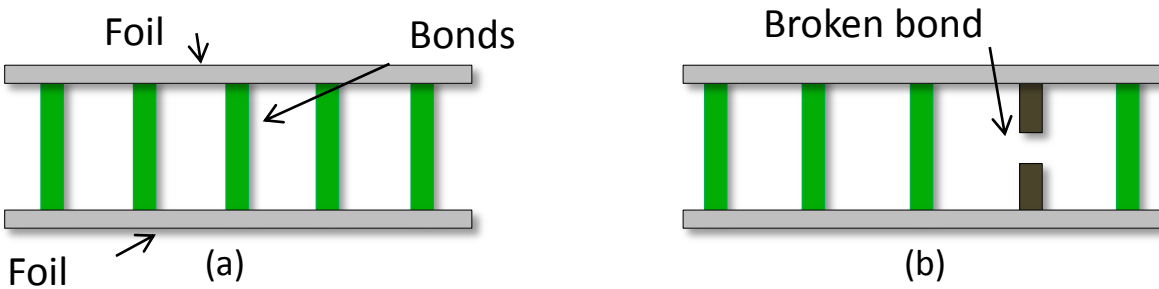


Figure 6 - Schematic of tensile loading and bond fracture for model theory showing a side view of the bonded foil layers at: (a) Initial bond conditions and (b) Bonding after a load cycle.

Table 2 - Model parameters for Frechet distribution.

Model Parameter	Value
s	3
σ_0	0.65, 0.80
α	5.25

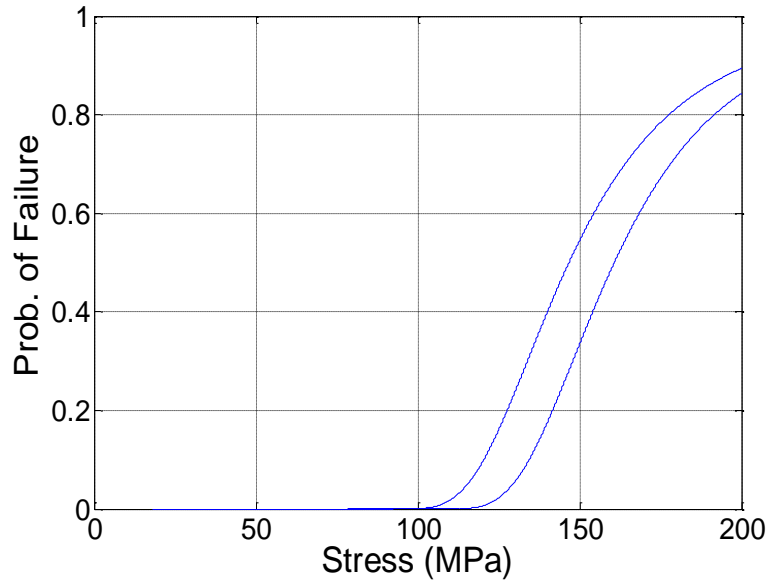


Figure 7 - Frechet curve [15] of failure probability for bonded areas.

This concept, and likewise the distribution, is similar to more commonly used techniques where a Weibull distribution is used to describe the probability of failure for a given material [16]. In this case however, each individual bond is investigated, instead of the failure of the part as a whole. For this model, the Frechet distribution was used because it provides an adequate description of the experimental fatigue data.

Model Results

The results of the model are shown with the experimental results in Figure 8. Ten simulations were performed at each of the experimentally tested stress values. The two samples that failed atypically, as described previously and found in Figure 2, were omitted as outliers. It is emphasized that the stress values reported are recalculated based on equation (2), accounting for the bonded area percentage as bearing the load. The results of the model show good correlation with the experimental results. Notably, the model accurately predicts the sample runout for the three sets of experiments run at less than 80 MPa (adjusted stress). These results indicate that the concept of probabilistic failure of bonded areas is a potentially suitable description of the behavior of low power UAM samples under dynamic loading conditions.

therefore be necessary to investigate the frequency with which these defects occur and determine how to limit their occurrence during processing.

In addition, a stress threshold of 50% of the UTTS was discovered below which failure did not occur within 3.75×10^7 cycles. This provides a lifetime prediction where, if these conditions are not exceeded, it is expected that a UAM component built with these process parameters would not fail.

Due to the lack of classic fatigue features in the failed specimens, a model was introduced to describe the failure as a simultaneous tensile loading of discretely bonded areas. The failure was modeled as a probability of failure using a Frechet distribution, whereby as the bonds in the UAM sample fail, the stress is redistributed and increased among the remaining bonds. The model shows a good correlation with the experimental results, providing an initial starting point for more refined methods to be applied to UAM bonded structures.

Acknowledgments

The authors would like to thank Dr. S. Suresh Babu of the Welding Engineering Program in the Department of Materials Science and Engineering at The Ohio State University for his assistance. Financial support for this research was provided by the member organizations of the Smart Vehicle Concepts Center (www.SmartVehicleCenter.org), a National Science Foundation Industry/University Cooperative Research Center.

References

- [1] K. Graff, "New Developments in Advanced Welding," Woodhead Publishing Limited, 2005.
- [2] D. White, "Ultrasonic consolidation of aluminum tooling," *Advanced materials & processes*, vol. 161, no. 1, pp. 64-65, 2003.
- [3] C. Kong, R. Soar and P. Dickens, "Optimum process parameters for ultrasonic consolidation of 3003 aluminum," *Journal of Materials Processing Technology*, vol. 146, no. 2, pp. 181-187, 2004.
- [4] E. Siggard, *Investigative research into the structural embedding of electrical and mechanical systems using ultrasonic consolidation*, Utah State University, Logan, UT: Masters Thesis, 2007.
- [5] C. Kong, R. Soar and P. Dickens, "Ultrasonic consolidation for embedding SMA fibres within aluminium matrices," *Composite Structures*, vol. 66, pp. 421-427, 2004.
- [6] C. H. Hopkins, M. J. Dapino and S. A. Fernandez, "Statistical Characterization of Ultrasonic Additive Manufacturing Ti/Al Composites," *Journal of Engineering Materials and Technology*, vol. 132, 2010.
- [7] R. Dehoff and S. Babu, "Characterization of interfacial microstructures in 3003 aluminum alloy blocks fabricated by ultrasonic additive manufacturing," *Acta Materialia*, pp. 1-12, 2010.
- [8] T. Friel, K. Johnson, P. Dickens and R. Harris, "The effect of interface topography for ultrasonic consolidation of aluminum," *Materials Science and Engineering A*, vol. 527, pp.

- 4474-4483, 2010.
- [9] M. Kulakov and H. Rack, "Control of 3003-H18 Aluminum Ultrasonic Consolidation," *Journal of Engineering Materials and Technology*, vol. 131, 2009.
- [10] C. H. Hopkins, P. J. Wolcott, M. J. Dapino, A. G. Truog, S. S. Babu and S. A. Fernandez, "Optimizing ultrasonic additive manufactured Al 3003 properties with statistical modeling," *Journal of Engineering Materials and Technology*, vol. 134, no. 1, 2012.
- [11] *ASTM E 466-07: Standard Practice for Conducting Force Controlled Constant Amplitude Axial Fatigue Tests of Metallic Materials*, ASTM International, 2007.
- [12] D. Schick, R. Hahnen, R. Dehoff, P. Collins, S. Babu, M. J. Dapino and J. Lippold, "Microstructural Characterization of Bonding Interfaces in Aluminum 3003 Blocks Fabricated by Ultrasonic Additive Manufacturing," *Welding Journal*, vol. 89, pp. 105-115, 2010.
- [13] T. Zhao and Y. Jiang, "Fatigue of 7075-T651 aluminum alloy," *International Journal of Fatigue*, vol. 30, pp. 834-849, 2008.
- [14] ASM-International, *Properties of Wrought Aluminum Alloys*, vol. 2, 2010.
- [15] E. Castillo, A. S. Hadi, N. Balakrishnan and J. M. Sarabia, *Extreme Value and Related Models with Applications in Engineering and Science*, Hoboken, N.J.: Wiley, 2005.
- [16] G. E. Dieter, *Mechanical Metallurgy*, McGraw-Hill Book Company, 1961.